

Interference Controls Conductance in Phthalocyanine Molecular Junctions

M. Teresa González,* Ali K. Ismael,* Miguel García-Iglesias, Edmund Leary, Gabino Rubio-Bollinger, Iain Grace, David González-Rodríguez, Tomás Torres, Colin J. Lambert, and Nicolás Agrait



Cite This: <https://doi.org/10.1021/acs.jpcc.1c03290>



Read Online

ACCESS |



Metrics & More

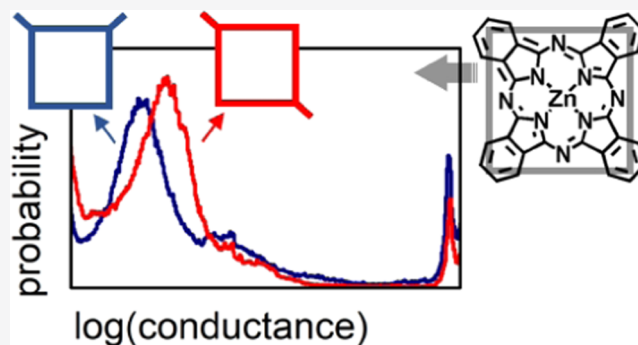


Article Recommendations



Supporting Information

ABSTRACT: We report an experimental and theoretical study of the single-molecule conductance of two separate families of regioisomeric phthalocyanine derivatives in which the binding groups are connected at opposite or at contiguous positions about the phthalocyanine moiety. We observe that compounds with the longest distance between the anchoring groups yield molecular junctions with a higher conductance compared to those with a shorter distance. We performed both density functional theory (DFT) and tight binding calculations to understand how interference effects explain the experimental results including the role of constructive and destructive quantum interference in five phthalocyanine derivatives.



INTRODUCTION

Phthalocyanine (Pc) molecules containing a central metal atom are commonly used as dyes and pigments. Within the field of organic electronics, they have great potential in device applications such as field-effect transistors,^{1,2} photovoltaic cells,^{3,4} optoelectronics,^{5,6} and spintronic devices.^{7,8} At the single-molecule level, Pcs have been studied using scanning tunneling microscopes (STMs)^{9,10} with the Pcs lying flat on various substrates,^{11–13} including graphene,^{14,15} so that transport occurs perpendicular to the molecule, usually through a tunnel barrier.^{16–18} In this configuration, phenomena such as the Kondo effect at low temperatures,^{19–22} magnetoresistance,^{23,24} spin switching,²⁵ or gas adsorption^{26,27} have been observed. On the other hand, there are only a few studies of transport properties in which the Pc is part of an individual molecular wire, attached to metallic electrodes at both ends. In a few examples, the Pc itself (without specific chemical anchoring groups) was trapped between two metallic electrodes.^{20,23} In contrast to Pcs, porphyrins have been much more widely studied in single-molecule-junction experiments,^{28–40} despite the fact that Pcs are generally more robust to degradation⁴¹ than porphyrins, which is an important advantage when considering future applications in the field of molecular electronics.

With regard to single-molecule conductance measurements, a structure of the form A_2B_2 is necessary, which comprises 2A units and 2B units either in an AABB or ABAB configuration. In this kind of molecule, the A or the B units should contain suitable functional groups (sulfides, amines, etc.) that can serve as anchor points to metal electrodes, thus facilitating the study

of the conductance across the π -conjugated skeleton. The reason for the previously mentioned preference of porphyrins over phthalocyanines in this field comes from the fact that the synthesis of AABB or ABAB macrocycles is far simpler for the former. This is clear from the wide number of well-established protocols to prepare unsymmetrically *meso*-substituted porphyrins, of which some are carried out in a stepwise manner, through the isolation of stable synthetic intermediates.^{42,43} That is not the case for phthalocyanines due to their different condensation chemistries and intrinsic structures. Synthetic protocols that lead to unsymmetrically substituted Pcs are scarce, many of them just limited to the use of steric effects between bulky phthalonitriles,⁴⁴ and certainly not universal and reliable for any kind of phthalonitrile combination.

In this work, by choosing an appropriate phthalonitrile combination, we have been able to synthesize two separate A_2B_2 phthalocyanine families, ABAB and AABB (Figure 1a) with metal-binding groups located on opposite or contiguous isoindole units, and study their single-molecule conductance properties individually. Two thiolated benzene rings located at different positions around the Pc ring serve as anchor groups to the tip and substrate of an STM to form single-molecule junctions under ambient conditions. Surprisingly, we observed

Received: April 12, 2021

Revised: June 10, 2021

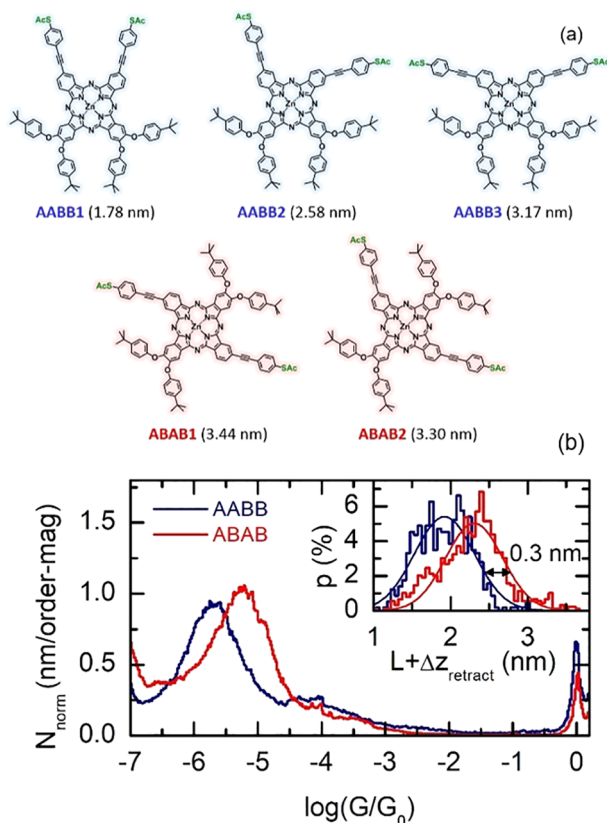


Figure 1. (a) Schematics of the studied molecules (expected molecular junction length in parentheses). (b) Conductance histograms obtained from several hundreds of G vs z traces for both groups. The inset in (b) shows the plateau-length distribution for each set of compounds.

higher conductance for the derivatives with binding groups located on opposite isoindole units of the Pcs (**ABAB** structures) than for those with binding groups on contiguous isoindole units (**AABB**), despite their longer through-bond and sulfur–sulfur length. Our density functional theory (DFT) calculations confirm this trend and show evidence of destructive quantum interference (QI) in some of the isomers. QI in the various isomers is explored in more detail using tight binding calculations.

EXPERIMENTAL SECTION

Synthesis. Chemicals were purchased from commercial suppliers and used without further purification. Solid, hygroscopic reagents were dried in a vacuum oven before use. Reaction solvents were thoroughly dried before using standard methods. MALDI-TOF-MS spectra were obtained from a Bruker Ultraflex III instrument equipped with a nitrogen laser operating at 337 nm. NMR spectra were recorded with a Bruker AC-400 (400 MHz). Chemical shifts are measured in ppm using the signals of the deuterated solvent as the internal standard. Column chromatography was carried out on silica gel Merck-60 (230–400 mesh, 60 Å), and TLC was carried out on aluminum sheets precoated with silica gel 60 F254 (E. Merck). UV/vis spectra were recorded with a JASCO V-660.

Conductance Measurements. We determined the single-molecule conductance of the Pc derivatives using a home-built scanning tunneling microscope (STM). Both the substrate

(commercial Arrandee substrates) and the tip (freshly cut 0.25 mm wires) of the STM were made of gold. The Pc derivatives were deposited by dip-casting using an approximately 1 mM solution in CH_2Cl_2 . Subsequently, all of the measurements were carried out with substrates in air after drying the solvent. We recorded G vs z traces by keeping a constant bias voltage of 200 mV between the tip and the substrate and recording the current while performing cycles of approach–retraction of the tip. A protection 1 M Ω resistor in series with the current circuit kept the current below 0.2 μA during the entire measurement. We use a linear current-to-voltage converter with two amplification stages of 4.3×10^7 and 8.8×10^9 V/A. To ensure a clean rupture of a broad gold contact during each cycle, an extra motion of 1–2 nm is performed when the conductance limits are reached both in the opening and closing. These limits were $1.5G_0$ during the closing and $2 \times 10^{-7}G_0$ (just above the experimental noise) during the closing.

Theoretical Details. To calculate the electronic properties and the electrical conductance of the molecules placed between gold electrodes, we used the SIESTA implementation of density functional theory (DFT),⁴⁵ combined with the GOLLUM code,⁴⁶ which is a newly developed quantum transport code. The optimum geometry of the isolated molecules was first calculated using DFT, with all forces on atoms relaxed to a tolerance of 0.01 V/Å. In all calculations, a double-zeta plus polarization (DZP) basis set, with norm-conserving pseudopotentials, was employed, and the Hamiltonian and overlap matrices were calculated on a real space grid defined by a plane wave cutoff of 200 Ry. After calculating the optimum geometry of the molecular wire, it was attached to gold electrodes. After removing the hydrogen atoms from the terminal thiol groups, the equilibrium distance between the S atom and a top atom on the surface of the gold electrode was found to be 2.2 Å. The gold electrodes consist of a pyramid of 11 gold atoms and six layers of (111) gold, with each layer containing 25 gold atoms. A Hamiltonian describing this structure was constructed using SIESTA, and then, GOLLUM was used to calculate the zero-bias transmission coefficients $T(E)$ describing electrons of energy E passing from one electrode to the other via the molecular wire. The electrical conductance was then related to the transmission through the Landauer formula $G = (2e^2/h) \times T(E_F)$.

RESULTS AND DISCUSSION

Pc-Derivate Synthesis. Different from porphyrins, for most phthalocyanines, the functional groups that allow for structural differentiation (A and B) must be placed at the 3- or 4-positions of the corresponding 1,2-dicyanobenzene precursors, which means that each of the A_3B , A_2B_2 , and AB_3 derivatives, if isolated, will be at the same time constituted by a mixture of isomers. For this reason, the synthesis of unsymmetrically substituted Pcs is usually carried out by statistical condensation of the two different phthalonitriles (A and B) followed by purification of the desired macrocycle by chromatography.⁴⁷ Needless to say, any other method for molecular separation, like recrystallization or sublimation, is useless for this purpose. Even if this protocol works efficiently for many phthalonitrile combinations, the inherent tendency of Pcs to aggregate by π – π stacking hampers strongly chromatographic separation at a reasonable scale. Hence, while the properties of “ A_3B (or AB_3)-type” Pcs have been extensively investigated for manifold applications, those of A_2B_2 derivatives

remain rather unexplored due to the great challenge in separating ABAB or AABB isomers.^{48–51}

We however found out here that isolation of the two desired A_2B_2 Pc isomers is facilitated by a combination of bulky, hydrophobic groups attached to the A unit, affording solubility and hampering aggregation, and polar groups placed on the B unit, which enhance the difference in polarity between the AABB and ABAB isomers during chromatographic separation. Specifically, condensation of 4,5-*tert*-butylphenoxyphthalonitrile and 4-(3-hydroxy-3-methyl-1-butynyl)phthalonitrile in the presence of $ZnCl_2$ led to a statistical mixture of Pcs from which the two isomers bearing the anchor groups either at the opposite (ABAB) or contiguous isoindol units (AABB) could be successfully isolated (see details in the Supporting Information). Then, the two unsymmetrically substituted Pcs were deprotected and end-capped with thioacetyl units, which serve as an anchor to ensure the formation of a robust Au–S bond to the gold electrodes, leading to final compounds ABAB and AABB. Each of these isomers is at the same time composed of a mixture of regioisomers shown in Figure 1a, which, unfortunately, is impossible to separate. While the ABAB sample comprises a 50–50% mixture of ABAB1 and ABAB2 regioisomers, the AABB sample is composed of a mixture of the AABB1, AABB2, and AABB3 regioisomers in a 25–50–25% ratio. The indicated percentage of regioisomers present in each sample was determined by 1H NMR spectroscopy and was in good agreement with the expected ratio based on purely statistical considerations. The separation of these two families of ABAB and AABB Pcs constitutes already an important milestone that allows the study of the single-molecule conductance across the core of this important class of molecular semiconductors, as has been done extensively for porphyrins.

Pc Molecular Junction Conductance. We studied the electrical transport properties of the Pc derivatives AABB and ABAB shown in Figure 1a using the break-junction technique. Performing thousands of retraction-approach cycles between the tip and substrate of our STM, we observed a very low probability of junction formation for these compounds, with percentages of retraction G vs z traces displaying regions of constant conductance (molecular plateaus) of around 2–3%. This compares with typical junction formation percentages in our own equivalent experiments of approximately 30% for an oligo(phenylene-ethynylene) dithiol with three phenyl units (OPE-3)⁵² or 17% for the porphyrin derivative counterpart,³⁷ both with the same thiophenyl terminal groups used here. A significant interaction between the phthalocyanine core and the electrode surface most probably reduces the molecular junction formation probability.

Each compound was studied in at least five independent measurement runs using new electrodes and molecular solutions to ensure reproducibility (see Figure S1). Gathering all recorded traces with plateaus, we built the one- and two-dimensional histograms shown in Figures 1b and 2a, respectively. A peak (cloud) is formed in the 1D (2D) histogram at the conductance values where many G vs z traces display plateaus. We determine the typical junction conductance for each compound as the mean value of these peaks: $\log(G/G_0)_{AABB} = -5.7$ and $\log(G/G_0)_{ABAB} = -5.2$, with a value of 0.5 for the half-width at half-maximum of the Gaussian fit to the peaks. It is significant that the conductance values of PC derivatives are lower than those observed previously for a

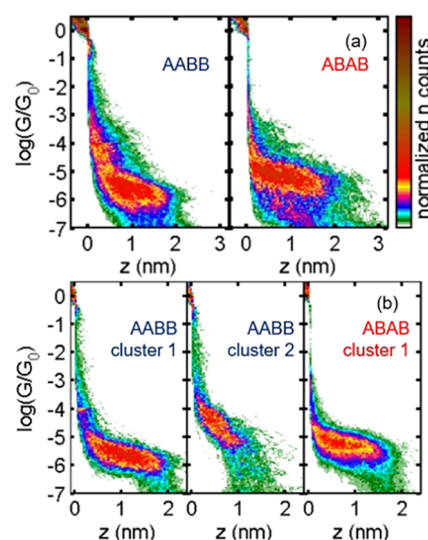


Figure 2. Two-dimensional conductance vs distance histograms corresponding to (a) all traces with plateaus (the same as in Figure 1b) and (b) traces in the main clusters identified by an automated algorithm (see the text for details).

similar porphyrin derivative³⁷ ($\log(G/G_0)_{\text{porph}} = -3.7$) and for OPE-3⁵² ($\log(G/G_0)_{\text{ope3}} = -3.9$).

Interestingly, despite their longer through-space distance between anchoring groups, the mean conductance of the ABAB derivatives is about half an order of magnitude higher than that of the AABB derivatives. By studying the independent runs separately, we obtained standard deviations from the mean values of 0.05 and 0.06 for the logarithm of the conductances of AABB and ABAB, respectively, reinforcing that the half-an-order-of-magnitude difference between the conductance of both compounds is significant and well above the measurement-to-measurement variation. Examples of conductance histograms of individual runs are shown in Figure S1. As shown in the plateau-length distributions of the inset to Figure 1b (considering only plateaus of the main peak), indeed the high-conductance ABAB plateaus are on average larger. At the right end of these distributions, which accounts for the longer junctions with molecules presumably fully elongated between the electrode apexes, we see a difference of 0.3 nm between AABB and ABAB, in good agreement with the difference in Figure 1a for the through-space distance between the anchoring groups of the longest regioisomers of each group (AABB3 and ABAB1). We therefore confirm that, for this family of compounds, the longest molecular junctions are the ones with higher conductance. We note here that throughout the family we are not changing the nature of the central part of the compounds but simply altering the position of the anchor groups. Significantly, this result differs from those obtained for closely related porphyrin derivatives, which display a lower conductance as the through-space distance between the binding groups increases.³¹ It is important to note that in that case the porphyrin core was contacted via the edges and not the corners as in the case of the Pc derivatives studied here. As we will see in the next section, the detailed position of the linkers in the molecular core plays a key role in determining electron transmission.

Theoretical Transport Calculations. To study the quantum transport properties of the five Pc isomers, we use the SIESTA implementation of density functional theory

(DFT),⁴⁵ combined with the GOLLUM code⁴⁶ (see Section 3 in the Supporting Information). This revealed that, for each of the isomers, the HOMO is delocalized across the entire molecule, while the LUMO lies mainly on the Pc core (see Figures S11–S15). As expected, the HOMO and LUMO energies are almost the same for all isomers, and only the geometric position of the anchor groups is changed. The fact that the orbitals are almost identical implies that any changes in the conductance are likely to be due to quantum interference (QI) effects^{53–65} mediated by the various transmission pathways through the molecule. We have also calculated the ionization potential for each isomer and found similar values of approximately 5.19 eV for each.

The isomers were contacted to two identical gold electrodes via their thiol anchor groups (Figure S16). The optimal binding distance between the tip of the gold and the sulfur atoms was found to be 0.23 nm. This leads to junctions with the Au–Au distances indicated in Figure 1a for the five isomers. The resulting transmission coefficients can be seen in Figure 3. Our results show that the transmission for all of the

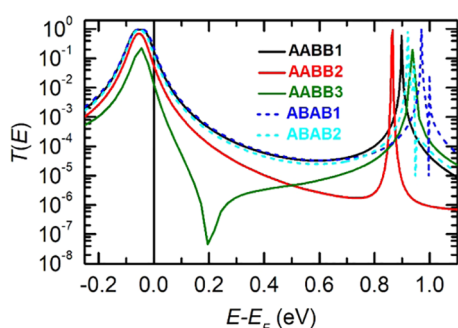


Figure 3. Calculated zero-bias transmission coefficient $T(E)$ obtained using DFT for the five different isomers.

isomers is dominated by HOMO, for which the Zn ion has practically no contribution. Figure 3 shows that for the ABAB isomers, the transmission at the DFT-predicted Fermi level ($E - E_F = 0$) is equal to or higher than that of the AABB isomers. In particular, the resulting conductance values are $G(E_F) = 0.17G_0$ for AABB1, $0.056G_0$ for AABB2, and $0.018G_0$ for AABB3, while isomers ABAB1 and ABAB2 possess similar transmission curves and have values of $0.23G_0$ and $0.13G_0$ at $E - E_F = 0$, respectively. Predicted conductance values are higher than those experimentally observed which is typical of DFT calculations. However, the overall conductance variation is well reproduced.

As anticipated, the results in Figure 3 show that AABB3 does possess a quantum interference dip near $E - E_F = 0.2$ eV, which reduces its transmission coefficient near the DFT-predicted Fermi energy. Since Pcs are planar aromatic macrocycles with extended π -systems, to explore the origin of this dip, we also performed extensive tight binding modeling of the five isomers (see Section 3.3 in the Supporting Information). We constructed a simple tight binding (i.e., Huckel) Hamiltonian, which describes the connectivity dependence of the electrical conductance of the Pc central unit, and deconstructed it in the equivalent lattice shown in Figures S19 and S21, exploring different connectivity parameters. Despite the apparent complexity of the Pc central unit, we found that a simple Hamiltonian based on connectivity alone reproduces many of the qualitative features

of the full DFT calculation, including the AABB3 interference dip. This dip is sensitive to the electronic coupling to the interior nitrogen atoms (Figure S20) and vanishes when this coupling is artificially set to zero. Therefore, in this study, the TBM proved to be more insightful than the DFT, bringing out the essential couplings causing the quantum interference dip. The comparison between the DFT and TBM calculations is shown in Figure S29.

Evaluation of Isomer Contributions to the Conductance Signal. Based on the above theoretical results, we explored whether we could identify the experimental signature of individual regioisomers contained in the experiments. For the ABAB series, the molecular junctions of ABAB1 and ABAB2 are predicted to have practically the same length and conductance; therefore, we would expect to observe a single conductance cloud accounting for both regioisomers. On the other hand, for the AABB series, the difference in length between regioisomers is between 0.6 and 1.4 nm, which could be experimentally separated, and the predicted conductance difference between the regioisomers of the highest and lowest conductances in Figure 3 is about one order of magnitude.

In Figure 2a, signals above $\log(G/G_0) = -4.5$ and below -6 (that is, above and below the main peak) can be seen. As shown in detail in the Supporting Information (Section 2.3), those below -6 are equally present for AABB and ABAB groups. As only one cloud is expected for the latter, we rule out these signals as signatures of different isomers also for AABB. They are probably produced by the less favorable binding configurations of the same regioisomers contributing to the main peak.^{38,66} Signals above -4.5 are also present in both groups but in quite different proportions, being more abundant for AABB, as is already evident in the 2D histograms of Figure 2a.

To explore in more detail the different plateau contributions to the histograms, we carried out an unsupervised k-means clustering subdivision of the measured conductance traces for both ABAB and AABB, similar to that found in the literature.^{38,67} Figure 2b collects the main clusters of traces relevant for our study, leaving out those signals common to both AABB and ABAB, which were discussed in the previous paragraph. A more detailed description of the clustering process and outcome is described in Section 2.4 of the Supporting Information. Figure 2b shows that, for AABB, a cluster of traces (cluster 2) is identified with plateaus on average 1 nm shorter and conductance one order of magnitude higher than the dominant one (cluster 1). Importantly, an equivalent set of traces was not observed for ABAB. Taking into account the results of the calculations in the previous section, these results are compatible with regioisomer AABB3 being responsible for the main conductance cloud in Figure 2a (cluster 1 of ABAB in Figure 2b), while the two other regioisomers AABB1 and AABB2 could be contributing to this minority set identified in the clustering subdivision (cluster 2 of ABAB in Figure 2b). Additional high-conductance plateaus observed for both sets of compounds could probably be caused by the direct binding of the Pc core to one of the electrodes. This configuration could easily be more favorable than the sulfur-to-sulfur link for AABB1. Less favorable bindings of the molecules with one electrode linked to some intermediate region different from the Pc core would also produce short plateaus, but these would presumably appear at lower conductance than the main one³⁸ and therefore could hardly account for the high-conductance plateaus described here.

Current vs Voltage Curves. We performed a new set of retraction-approach cycles recording current–voltage (*IV*) curves at different *z* positions along the conductance plateaus (see the Supporting Information for details). Figure 4a shows

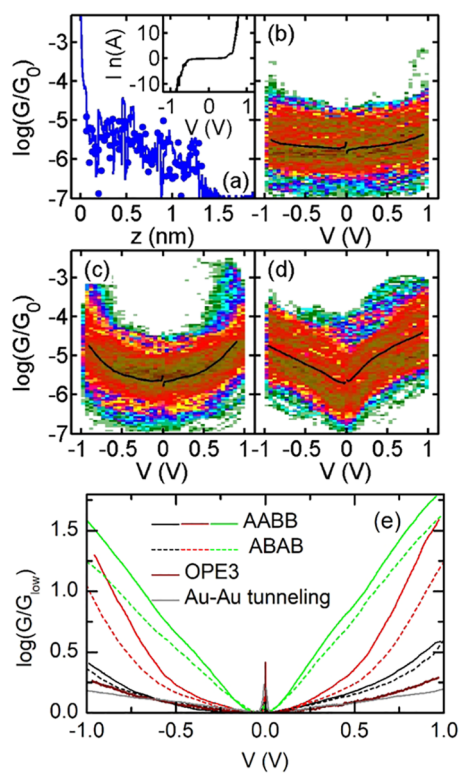


Figure 4. (a) Example of a *G* vs *z* trace with recorded *IV* curves along the conductance plateau. The averaged *IV* curve along the plateau is shown in the inset. (b)–(d) 2D histograms of all of the *G* vs *V* curves for a measurement run with the ABAB derivative. The curves have been divided into groups according to their overall profile as flat (b), U-shape (c), and V-shape (d). (e) Comparison of the averaged *G* vs *V* profiles for AABB and ABAB.

an example of the results for one *G* vs *z* trace, where the positions at which *IV* curves were recorded are marked with solid circles, and the average *IV* along the plateau is displayed in the inset. Figure 4b–d shows the statistical study of all of the recorded curves for ABAB, where we defined the conductance to be $G = I/V$. Significantly, we were able to distinguish three different general curve profiles: flat (4b), U-shape (4c), and V-shape (4d). The separation into these three groups was carried out visually and is not intended to be an exhaustive statistical study. Rather, it allows us to describe the differing observed molecular behavior. While we identified changes in the profile along some of the conductance plateaus (see Figures S9 and S10), for the sake of simplicity, the whole set of *GV* curves of one plateau was placed into a single group in the separation of Figure 4.

In Figure 4e, we compare the averaged *GV* curves of both Pc derivatives (normalized to their conductance in the interval ± 0.05 V, G_{low}) with those recorded without molecules (gold-to-gold tunneling) and for the OPE-3 dithiol reference. We see that the latter only produces “flat” *GV* curves with a profile similar to that of Figure 4b but never displays the strong dependence with bias voltage observed in Figure 4c,d (see also Figures S7 and S8 in the Supporting Information). In addition, the increase in conductance with the bias voltage is

systematically larger for the AABB derivative than for the ABAB one, independently of the *GV* profile.

The flat and “V-shape” profiles of Figure 4b,d are very similar to those reported previously for dithiol and monothiol anthraquinone derivatives.⁵⁷ There, the V-shape was explained by the presence of an “antiresonance” dip quite close to the Fermi level for the monothiol derivative. Here, we observed three types of curves for the same compound. While we have a mixture of different regioisomers for each Pc derivative, which could be the origin of the different *GV* profiles, we note that the same three profiles were found for both Pc derivatives (see Figure 4e). In Figure 3, we see that AABB3 displays a strong dip in the HOMO–LUMO gap, but none of the regioisomers of ABAB exhibit such a dip, so we would not expect V-shape *GV* curves arising from destructive quantum interference for this group.

The above-mentioned changes from one profile to another during the elongation of individual molecular junctions (Figures S9 and S10) strongly suggest that the different *GV* profiles are not due to different regioisomers but rather a change in the state of an individual molecule or its binding to the electrodes. In fact, we have recently reported very similar *GV* profiles and profile switches for similar porphyrin-based molecular junctions,⁶⁸ which become charged at high bias within the junction. The similarities of the results presented here to those of the porphyrin derivatives suggest that the Pc molecules are also changing their charge state, this being behind the different profiles in Figure 4. We also observed that the percentage of molecular junctions producing each type of profile was quite variable for different experimental runs, which suggests that the geometry of the tip or the density of molecules around the electrodes plays an important role. We speculate that some arrangements can promote coupling of the central phthalocyanine to the electrodes, thus modifying the transmission profile. There are also variations in the percentage of plateaus that show a *GV* profile for the two studied compounds. While for AABB, the V-shape is the most frequent (appearing in 50–85% of the *G* vs *z* traces in different experimental runs), the “U-shape” is dominant for ABAB (40–75% of the traces).

Outlook. Recently, it has become clear that molecules containing heteroatoms modulate QI effects in unique ways. Garner et al. showed that certain chemical substituents, such as halogens, amino, or alkoxy groups, placed on the central ring of a *meta*-connected OPE-3 change the energetic position of the interference features quite dramatically.⁶⁹ Liu et al. showed that substituting carbon for nitrogen in the same *meta*-OPE-3 structure also produces a similar effect.⁷⁰ Comparisons also between fluorene and fluorenone molecular wires have further highlighted the special relation between QI and the presence of heteroatoms.⁷¹ Meanwhile, Zotti et al. showed that the energetic shift produced by the substituents could be decomposed into the chemical resonance and inductive contributions of the substituent.⁷² In the case of Pcs, the central ring contains eight nitrogen atoms, four of which coordinate to a metal ion. Modulating the onsite energy of the central nitrogens has a dramatic effect on the position of the antiresonance (see Section 3.3 of the Supporting Information), in accordance with the effects described previously. This therefore strongly suggests that if one can modify the electronic environment of these atoms, one would have a direct handle on the interference features. We propose that changing the metal ion could do just this. Pcs can be prepared

with a wide range of metals (Zn, Cu, and Co, for example), meaning that there is plenty of scope to test this possibility. Furthermore, the substituents attached to the perimeter of the Pc can also be changed, which means that compared to the typical OPE-3 structure, Pcs represent a significantly more promising candidate structure with which to tune QI features in an exquisite and unprecedented manner to produce sought-after properties. This remains a fertile ground for further exploration.

Conclusions. In summary, we have been able to separate two phthalocyanine AABB and ABAB families with binding groups at different positions around the phthalocyanine core and have studied their single-molecule junction electrical properties. Experimentally, we found that isomers with anchoring groups located at opposite isoindol units of the phthalocyanine, ABAB, yield higher conductance than those with anchoring groups at contiguous isoindol units, AABB. This means that molecules with a larger through-bond pathway conduct better than those with correspondingly shorter paths. In agreement with these results, our DFT calculations predict higher transmission for the ABAB derivatives compared to that for AABB. We find that the lower conductance of AABB3 is due to the presence of a dip in the transmission curve near the Fermi level of the electrodes due to quantum interference, which tight binding modeling reveals arises from the electronic coupling to the interior nitrogens of the phthalocyanine. Strong dependence of the conductance with the voltage was observed for both groups. Our results shed light on the unexplored single-molecule conductance of this important class of π -conjugated molecular materials and, in particular, on the subtle differences of through-bond conductance pathways in molecular electronics.

■ ASSOCIATED CONTENT

SI Supporting Information

The Supporting Information is available free of charge at <https://pubs.acs.org/doi/10.1021/acs.jpcc.1c03290>.

Synthetic procedures and characterization; data analysis including the characterization of minority peaks, clustering analysis, and current–voltage curve analysis; theoretical calculation details including the schematics of the frontier orbitals and molecular junction geometries of the studied compounds; and tight binding study of the interference in the phthalocyanine derivatives (PDF)

■ AUTHOR INFORMATION

Corresponding Authors

M. Teresa González – *Fundación IMDEA Nanociencia, Ciudad Universitaria de Cantoblanco, E-28049 Madrid, Spain*; orcid.org/0000-0002-7253-797X;
Email: teresa.gonzalez@imdea.org

Ali K. Ismael – *Department of Physics, Lancaster University, Lancaster LA1 4YB, England; Department of Physics, College of Education for Pure Science, Tikrit University, Tikrit 34001, Iraq*; orcid.org/0000-0001-7943-3519;
Email: k.ismael@lancaster.ac.uk

Authors

Miguel García-Iglesias – *Fundación IMDEA Nanociencia, Ciudad Universitaria de Cantoblanco, E-28049 Madrid, Spain; Departamento de Química Orgánica, Universidad Autónoma de Madrid, E-28049 Madrid, Spain*; Present

Address: Department of QUIPRE, Inorganic Chemistry-University of Cantabria, 39005 Santander, Spain;

orcid.org/0000-0001-6359-9020

Edmund Leary – *Fundación IMDEA Nanociencia, Ciudad Universitaria de Cantoblanco, E-28049 Madrid, Spain*;

orcid.org/0000-0001-7541-5997

Gabino Rubio-Bollinger – *Departamento de Física de la Materia Condensada, Condensed Matter Physics Center (IFIMAC), and Instituto "Nicolás Cabrera", Universidad Autónoma de Madrid, E-28049 Madrid, Spain*;

orcid.org/0000-0001-7864-8980

Iain Grace – *Department of Physics, Lancaster University, Lancaster LA1 4YB, England*

David González-Rodríguez – *Departamento de Química Orgánica, Universidad Autónoma de Madrid, E-28049 Madrid, Spain; Institute for Advanced Research in Chemical Sciences (IAdChem), Universidad Autónoma de Madrid, 28049 Madrid, Spain*; orcid.org/0000-0002-2651-4566

Tomás Torres – *Fundación IMDEA Nanociencia, Ciudad Universitaria de Cantoblanco, E-28049 Madrid, Spain; Departamento de Química Orgánica, Universidad Autónoma de Madrid, E-28049 Madrid, Spain; Institute for Advanced Research in Chemical Sciences (IAdChem), Universidad Autónoma de Madrid, 28049 Madrid, Spain; IRLON, Research Institute of Macrocyclics, Ivanovo State University of Chemistry and Technology, Ivanovo Oblast 153000 Ivanovo, Russia*; orcid.org/0000-0001-9335-6935

Colin J. Lambert – *Department of Physics, Lancaster University, Lancaster LA1 4YB, England*; orcid.org/0000-0003-2332-9610

Nicolás Agraït – *Fundación IMDEA Nanociencia, Ciudad Universitaria de Cantoblanco, E-28049 Madrid, Spain; Departamento de Física de la Materia Condensada, Condensed Matter Physics Center (IFIMAC), and Instituto "Nicolás Cabrera", Universidad Autónoma de Madrid, E-28049 Madrid, Spain*; orcid.org/0000-0003-4840-5851

Complete contact information is available at:
<https://pubs.acs.org/doi/10.1021/acs.jpcc.1c03290>

Notes

The authors declare no competing financial interest.

■ ACKNOWLEDGMENTS

A.K.I. acknowledges the Leverhulme Trust for Early Career Fellowship ECF-2020-638 and financial support from Tikrit University (Iraq), the Iraqi Ministry of Higher Education (SL-20). A.K.I. and C.J.L. acknowledge financial support from the UK EPSRC through grant nos. EP/M014452/1, EP/P027156/1, and EP/N03337X/1. This work was additionally supported by the European Commission through the FET Open project 767187-QuIET. This work was supported by Spanish MICINN (MAT2017-88693-R, CTQ2017-85393-P, CTQ2017-84727-P, and PID2020-116490GB-I00). Support from the UK EPSRC is acknowledged through grant nos. EP/N017188/1, EP/M014452/1, EP/P027156/1, and EP/N03337X/1. IMDEA Nanociencia acknowledges support from the “Severo Ochoa” Programme for Centres of Excellence in R&D (MINECO, grant SEV2016-0686). The authors thank the Comunidad de Madrid Atracción de Talento grant 2019-T1/IND-16384 (EL) and NanoMagCOST (CM S2018/NMT-4321). N.A. and G.R.B. acknowledge financial support

from the Spanish Ministry of Science and Innovation through the “María de Maeztu” Programme for Units of Excellence in R&D (CEX2018-000805-M).

REFERENCES

- (1) Bao, Z.; Lovinger, A. J.; Dodabalapur, A. Organic Field-effect Transistors with High Mobility Based on Copper Phthalocyanine. *Appl. Phys. Lett.* **1996**, *69*, 3066–3068.
- (2) Gsänger, M.; Bialas, D.; Huang, L.; Stolte, M.; Würthner, F. Organic Semiconductors Based on Dyes and Color Pigments. *Adv. Mater.* **2016**, *28*, 3615–3645.
- (3) Satake, A.; Kobuke, Y. Artificial Photosynthetic Systems: Assemblies of Slipped Cofacial Porphyrins and Phthalocyanines Showing Strong Electronic Coupling. *Org. Biomol. Chem.* **2007**, *5*, 1679–1691.
- (4) Wang, Y.; Liu, X.; Shan, H.; Chen, Q.; Liu, T.; Sun, X.; Ma, D.; Zhang, Z.; Xu, J.; Xu, Z. X. Tetra-Alkyl-Substituted Copper (II) Phthalocyanines as Dopant-Free Hole-Transport Layers for Planar Perovskite Solar Cells with Enhanced Open Circuit Voltage and Stability. *Dyes Pigm.* **2017**, *139*, 619–626.
- (5) Das, P.; Chakraborty, K.; Chakrabarty, S.; Ghosh, S.; Pal, T. Reduced Graphene Oxide - Zinc Phthalocyanine Composites as Fascinating Material for Optoelectronic and Photocatalytic Applications. *ChemistrySelect* **2017**, *2*, 3297–3305.
- (6) Choi, S. A.; Kim, K.; Jin Lee, S.; Lee, H.; Babajanyan, A.; Friedman, B.; Lee, K. Effects of Thermal Preparation on Copper Phthalocyanine Organic Light Emitting Diodes. *J. Lumin.* **2016**, *171*, 149–153.
- (7) Jiang, S. W.; Wang, P.; Chen, B. B.; Zhou, Y.; Ding, H. F.; Wu, D. Tuning Carrier Mobility without Spin Transport Degrading in Copper-Phthalocyanine. *Appl. Phys. Lett.* **2015**, *107*, No. 042407.
- (8) Barraud, C.; Bouzehouane, K.; Deranlot, C.; Kim, D. J.; Rakshit, R.; Shi, S.; Arabski, J.; Bowen, M.; Beaurepaire, E.; Boukari, S.; et al. Phthalocyanine Based Molecular Spintronic Devices. *Dalton Trans.* **2016**, *45*, 16694–16699.
- (9) Gottfried, J. M. Surface Chemistry of Porphyrins and Phthalocyanines. *Surf. Sci. Rep.* **2015**, *70*, 259–379.
- (10) Li, Z.; Li, B.; Yang, J.; Hou, J. G. Single-Molecule Chemistry of Metal Phthalocyanine on Noble Metal Surfaces. *Acc. Chem. Res.* **2010**, *43*, 954–962.
- (11) Nakashima, S.; Yamagishi, Y.; Oiso, K.; Yamada, T. K. How Contacting Electrodes Affect Single π -Conjugated Molecular Electronic States: Local Density of States of Phthalocyanine Nanomolecules on MgO(001), Cu(111), Ag(001), Fe(001), and Mn(001). *Jpn. J. Appl. Phys.* **2013**, *52*, No. 110115.
- (12) Praznner-Bechcicki, J. S.; Zajac, L.; Olszowski, P.; Jöhr, R.; Hinaut, A.; Glatzel, T.; Such, B.; Meyer, E.; Szymonski, M. Scanning Probe Microscopy Studies on the Adsorption of Selected Molecular Dyes on Titania. *Beilstein J. Nanotechnol.* **2016**, *7*, 1642–1653.
- (13) Wu, R.; Yan, L.; Bao, D. L.; Ren, J.; Du, S.; Wang, Y.; Huan, Q.; Gao, H. J. Self-Assembly Evolution of Metal-Free Naphthalocyanine Molecules on Ag(111) at the Submonolayer Coverage. *J. Phys. Chem. C* **2019**, *123*, 7202–7208.
- (14) Bazarnik, M.; Brede, J.; Decker, R.; Wiesendanger, R. Tailoring Molecular Self-Assembly of Magnetic Phthalocyanine Molecules on Fe- and Co-Intercalated Graphene. *ACS Nano* **2013**, *7*, 11341–11349.
- (15) Uihlein, J.; Polek, M.; Glaser, M.; Adler, H.; Ovsyannikov, R.; Bauer, M.; Ivanovic, M.; Preobrajenski, A. B.; Generalov, A. V.; Chassé, T.; et al. Influence of Graphene on Charge Transfer between CoPc and Metals: The Role of Graphene–Substrate Coupling. *J. Phys. Chem. C* **2015**, *119*, 15240–15247.
- (16) Wu, S. W.; Nazin, G. V.; Chen, X.; Qiu, X. H.; Ho, W. Control of Relative Tunneling Rates in Single Molecule Bipolar Electron Transport. *Phys. Rev. Lett.* **2004**, *93*, No. 236802.
- (17) Nazin, G. V.; Wu, S. W.; Ho, W. Tunneling Rates in Electron Transport through Double-Barrier Molecular Junctions in a Scanning Tunneling Microscope. *Proc. Natl. Acad. Sci. U.S.A.* **2005**, *102*, 8832–8837.
- (18) Karan, S.; Jacob, D.; Karolak, M.; Hamann, C.; Wang, Y.; Weismann, A.; Lichtenstein, A. I.; Berndt, R. Shifting the Voltage Drop in Electron Transport Through a Single Molecule. *Phys. Rev. Lett.* **2015**, *115*, No. 016802.
- (19) Zhao, A.; Li, Q.; Chen, L.; Xiang, H.; Wang, W.; Pan, S.; Wang, B.; Xiao, X.; Yang, J.; Hou, J. G.; et al. Controlling the Kondo Effect of an Adsorbed Magnetic Ion Through Its Chemical Bonding. *Science* **2005**, *309*, 1542–1544.
- (20) Rakhmievitch, D.; Korytár, R.; Bagrets, A.; Evers, F.; Tal, O. Electron-Vibration Interaction in the Presence of a Switchable Kondo Resonance Realized in a Molecular Junction. *Phys. Rev. Lett.* **2014**, *113*, No. 236603.
- (21) Minamitani, E.; Fu, Y. S.; Xue, Q. K.; Kim, Y.; Watanabe, S. Spatially Extended Underscreened Kondo State from Collective Molecular Spin. *Phys. Rev. B: Condens. Matter Phys.* **2015**, *92*, 1–5.
- (22) Kügel, J.; Karolak, M.; Krönlein, A.; Senkpiel, J.; Hsu, P.-J.; Sangiovanni, G.; Bode, M. State Identification and Tunable Kondo Effect of MnPc on Ag(001). *Phys. Rev. B* **2015**, *91*, No. 235130.
- (23) Schmaus, S.; Bagrets, A.; Nahas, Y.; Yamada, T. K.; Bork, A.; Bowen, M.; Beaurepaire, E.; Evers, F.; Wulfhekel, W. Giant Magnetoresistance through a Single Molecule. *Nat. Nanotechnol.* **2011**, *6*, 185–189.
- (24) Warner, B.; El Hallak, F.; Prüser, H.; Sharp, J.; Persson, M.; Fisher, A. J.; Hirjibehedin, C. F. Tunable Magnetoresistance in an Asymmetrically Coupled Single-Molecule Junction. *Nat. Nanotechnol.* **2015**, *10*, 259–263.
- (25) Kügel, J.; Karolak, M.; Krönlein, A.; Serrate, D.; Bode, M.; Sangiovanni, G. Reversible Magnetic Switching of High-Spin Molecules on a Giant Rashba Surface. *npj Quantum Mater.* **2018**, *3*, No. 53.
- (26) Zhang, J. L.; Wang, Z.; Zhong, J. Q.; Yuan, K. D.; Shen, Q.; Xu, L. L.; Niu, T. C.; Gu, C. D.; Wright, C. A.; Tadich, A.; et al. Single-Molecule Imaging of Activated Nitrogen Adsorption on Individual Manganese Phthalocyanine. *Nano Lett.* **2015**, *15*, 3181–3188.
- (27) Zhong, J. Q.; Wang, Z.; Zhang, J. L.; Wright, C. A.; Yuan, K.; Gu, C.; Tadich, A.; Qi, D.; Li, H. X.; Lai, M.; et al. Reversible Tuning of Interfacial and Intramolecular Charge Transfer in Individual MnPc Molecules. *Nano Lett.* **2015**, *15*, 8091–8098.
- (28) Sedghi, G.; Sawada, K.; Esdaile, L. J.; Hoffmann, M.; Anderson, H. L.; Bethell, D.; Haiss, W.; Higgins, S. J.; Nichols, R. J. Single Molecule Conductance of Porphyrin Wires with Ultralow Attenuation. *J. Am. Chem. Soc.* **2008**, *130*, 8582–8583.
- (29) Qian, G.; Saha, S.; Lewis, K. M. Two-State Conductance in Single Zn Porphyrin Molecular Junctions. *Appl. Phys. Lett.* **2010**, *96*, No. 243107.
- (30) Perrin, M. L.; Martin, C. A.; Prins, F.; Shaikh, A. J.; Eelkema, R.; van Esch, J. H.; Van Ruitenbeek, J. M.; van der Zant, H. S. J.; Dulić, D. Charge Transport in a Zinc–Porphyrin Single-Molecule Junction. *Beilstein J. Nanotechnol.* **2011**, *2*, 714–719.
- (31) Li, Z.; Borguet, E. Determining Charge Transport Pathways through Single Porphyrin Molecules Using Scanning Tunneling Microscopy Break Junctions. *J. Am. Chem. Soc.* **2012**, *134*, 63–66.
- (32) Li, Z.; Park, T.-H.; Rawson, J.; Therien, M. J.; Borguet, E. Quasi-Ohmic Single Molecule Charge Transport through Highly Conjugated Meso-to-Meso Ethyne-Bridged Porphyrin Wires. *Nano Lett.* **2012**, *12*, 2722–2727.
- (33) Li, Z.; Smeu, M.; Ratner, M. A.; Borguet, E. Effect of Anchoring Groups on Single Molecule Charge Transport through Porphyrins. *J. Phys. Chem. C* **2013**, *117*, 14890–14898.
- (34) Aragonès, A. C.; Darwish, N.; Saletta, W. J.; Pérez-García, L.; Sanz, F.; Puigmartí-Luis, J.; Amabilino, D. B.; Díez-Pérez, I. Highly Conductive Single-Molecule Wires with Controlled Orientation by Coordination of Metalloporphyrins. *Nano Lett.* **2014**, *14*, 4751–4756.
- (35) Liu, Z.-F.; Wei, S.; Yoon, H.; Adak, O.; Ponce, I.; Jiang, Y.; Jang, W.-D.; Campos, L. M.; Venkataraman, L.; Neaton, J. B. Control

of Single-Molecule Junction Conductance of Porphyrins via a Transition-Metal Center. *Nano Lett.* **2014**, *14*, 5365–5370.

(36) Leary, E.; Roche, C.; Jiang, H. W.; Grace, I.; González, M. T.; Rubio-Bollinger, G.; Romero-Muñiz, C.; Xiong, Y.; Al-Galiby, Q.; Noori, M.; et al. Detecting Mechanochemical Atropisomerization within an STM Break Junction. *J. Am. Chem. Soc.* **2018**, *140*, 710–718.

(37) Leary, E.; Limburg, B.; Alanazy, A.; Sangtarash, S.; Grace, I.; Swada, K.; Esdaile, L. J.; Noori, M.; González, M. T.; Rubio-Bollinger, G.; et al. Bias-Driven Conductance Increase with Length in Porphyrin Tapes. *J. Am. Chem. Soc.* **2018**, *140*, 12877–12883.

(38) El Abbassi, M.; Zwick, P.; Rates, A.; Stefani, D.; Prescimone, A.; Mayor, M.; van der Zant, H. S. J.; Dulić, D. Unravelling the Conductance Path through Single-Porphyrin Junctions. *Chem. Sci.* **2019**, *10*, 8299–8305.

(39) Handayani, M.; Tanaka, H.; Katayose, S.; Ohto, T.; Chen, Z.; Yamada, R.; Tada, H.; Ogawa, T. Three Site Molecular Orbital Controlled Single-Molecule Rectifiers Based on Perpendicularly Linked Porphyrin-Imide Dyads. *Nanoscale* **2019**, *11*, 22724–22729.

(40) Aragonès, A. C.; Martín-Rodríguez, A.; Aravena, D.; Puigmartí-Luis, J.; Amabilino, D. B.; Aliaga-Alcalde, N.; González-Campo, A.; Ruiz, E.; Díez-Pérez, I. Tuning Single-Molecule Conductance in Metalloporphyrin-Based Wires via Supramolecular Interactions. *Angew. Chem. Int. Ed.* **2020**, *59*, 19193–19201.

(41) Kadish, K. M.; Smith, K. M.; Guillard, R. *Handbook of Porphyrin Science*; World Scientific: Singapore, 2010.

(42) Urbani, M.; Grätzel, M.; Nazeeruddin, M. K.; Torres, T. Meso-Substituted Porphyrins for Dye-Sensitized Solar Cells. *Chem. Rev.* **2014**, *114*, 12330–12396.

(43) Vicente, M.; Smith, K. Syntheses and Functionalizations of Porphyrin Macrocycles. *Curr. Org. Synth.* **2014**, *11*, 3–28.

(44) Fazio, E.; Jaramillo-García, J.; De La Torre, G.; Torres, T. Efficient Synthesis of ABAB Functionalized Phthalocyanines. *Org. Lett.* **2014**, *16*, 4706–4709.

(45) Soler, J. M.; Artacho, E.; Gale, J. D.; García, A.; Junquera, J.; Ordejón, P.; Sánchez-Portal, D. The SIESTA Method for Ab Initio Order-N Materials Simulation. *J. Phys. Condens. Matter* **2002**, *14*, 2745–2779.

(46) Ferrer, J.; Lambert, C. J.; García-Suárez, V. M.; Manrique, D. Z.; Visontai, D.; Oroszlany, L.; Rodríguez-Ferradás, R.; Grace, I.; Bailey, S. W. D.; Gillemot, K.; et al. GOLLUM: A next-Generation Simulation Tool for Electron, Thermal and Spin Transport. *New J. Phys.* **2014**, *16*, No. 093029.

(47) de la Torre, G.; Bottari, G.; Hahn, U.; Torres, T. Functional Phthalocyanines: Synthesis, Nanostructuring, and Electro-Optical Applications. In *Structure and Bonding*, 2010; Vol. 135, pp 1–44.

(48) de la Torre, G.; Claessens, C. G.; Torres, T. Phthalocyanines: The Need for Selective Synthetic Approaches. *European J. Org. Chem.* **2000**, *2000*, 2821–2830.

(49) Kobayashi, N.; Miwa, H.; Nemykin, V. N. Adjacent versus Opposite Type Di-Aromatic Ring-Fused Phthalocyanine Derivatives: Synthesis, Spectroscopy, Electrochemistry, and Molecular Orbital Calculations. *J. Am. Chem. Soc.* **2002**, *124*, 8007–8020.

(50) Haas, M.; Liu, S. X.; Neels, A.; Decurtins, S. A Synthetic Approach to Asymmetric Phthalocyanines with Peripheral Metal-Binding Sites. *European J. Org. Chem.* **2006**, *2006*, 5467–5478.

(51) Ranta, J.; Kumpulainen, T.; Lemmetyinen, H.; Efimov, A. Synthesis and Characterization of Monoisomeric 1,8,15,22-Substituted (A3B and A2B2) Phthalocyanines and Phthalocyanine-Fullerene Dyads. *J. Org. Chem.* **2010**, *75*, 5178–5194.

(52) González, M. T.; Leary, E.; García, R.; Verma, P.; Herranz, M. A.; Rubio-Bollinger, G.; Martín, N.; Agrait, N. Break-Junction Experiments on Acetyl-Protected Conjugated Dithiols under Different Environmental Conditions. *J. Phys. Chem. C* **2011**, *115*, 17973–17978.

(53) Vazquez, H.; Skouta, R.; Schneebeli, S.; Kamenetska, M.; Breslow, R.; Venkataraman, L.; Hybertsen, M. S. Probing the Conductance Superposition Law in Single-Molecule Circuits with Parallel Paths. *Nat. Nanotechnol* **2012**, *7*, 663–667.

(54) Ballmann, S.; Härtle, R.; Coto, P. B.; Elbing, M.; Mayor, M.; Bryce, M. R.; Thoss, M.; Weber, H. B. Experimental Evidence for Quantum Interference and Vibrationally Induced Decoherence in Single-Molecule Junctions. *Phys. Rev. Lett.* **2012**, *109*, No. 056801.

(55) Aradhya, S. V.; Meisner, J. S.; Krikorian, M.; Ahn, S.; Parameswaran, R.; Steigerwald, M. L.; Nuckolls, C.; Venkataraman, L. Dissecting Contact Mechanics from Quantum Interference in Single-Molecule Junctions of Stilbene Derivatives. *Nano Lett.* **2012**, *12*, 1643–1647.

(56) Kaliginedi, V.; Moreno-García, P.; Valkenier, H.; Hong, W.; García-Suárez, V. M.; Buitter, P.; Otten, J. L. H.; Hummelen, J. C.; Lambert, C. J.; Wandlowski, T. Correlations between Molecular Structure and Single-Junction Conductance: A Case Study with Oligo(Phenylene-Ethynylene)-Type Wires. *J. Am. Chem. Soc.* **2012**, *134*, S262–S275.

(57) Guédon, C. M.; Valkenier, H.; Markussen, T.; Thygesen, K. S.; Hummelen, J. C.; Van Der Molen, S. J. Observation of Quantum Interference in Molecular Charge Transport. *Nat. Nanotechnol.* **2012**, *7*, 305–309.

(58) Arroyo, C. R.; Tarkuc, S.; Frisenda, R.; Seldenthuis, J. S.; Woerde, C. H. M.; Eelkema, R.; Grozema, F. C.; van der Zant, H. S. J. Signatures of Quantum Interference Effects on Charge Transport Through a Single Benzene Ring. *Angew. Chem.* **2013**, *125*, 3234–3237.

(59) Xia, J.; Capozzi, B.; Wei, S.; Strange, M.; Batra, A.; Moreno, J. R.; Amir, R. J.; Amir, E.; Solomon, G. C.; Venkataraman, L.; et al. Breakdown of Interference Rules in Azulene, a Nonalternant Hydrocarbon. *Nano Lett.* **2014**, *14*, 2941–2945.

(60) Sangtarash, S.; Huang, C.; Sadeghi, H.; Sorohov, G.; Hauser, J.; Wandlowski, T.; Hong, W.; Decurtins, S.; Liu, S.-X.; Lambert, C. J. Searching the Hearts of Graphene-like Molecules for Simplicity, Sensitivity, and Logic. *J. Am. Chem. Soc.* **2015**, *137*, 11425–11431.

(61) Geng, Y.; Sangtarash, S.; Huang, C.; Sadeghi, H.; Fu, Y.; Hong, W.; Wandlowski, T.; Decurtins, S.; Lambert, C. J.; Liu, S.-X. Magic Ratios for Connectivity-Driven Electrical Conductance of Graphene-like Molecules. *J. Am. Chem. Soc.* **2015**, *137*, 4469–4476.

(62) Manrique, D. Z.; Huang, C.; Baghernejad, M.; Zhao, X.; Al-Owaedi, O. A.; Sadeghi, H.; Kaliginedi, V.; Hong, W.; Gulcur, M.; Wandlowski, T.; et al. Quantum Circuit Rule for Interference Effects in Single-Molecule Electrical Junctions. *Nat. Commun.* **2015**, *6*, No. 6389.

(63) Gantenbein, M.; Wang, L.; Al-Jobory, A. A.; Ismael, A. K.; Lambert, C. J.; Hong, W.; Bryce, M. R. Quantum Interference and Heteroaromaticity of Para- and Meta-Linked Bridged Biphenyl Units in Single Molecular Conductance Measurements. *Sci. Rep.* **2017**, *7*, No. 1794.

(64) Ismael, A. K.; Grace, I.; Lambert, C. J. Connectivity Dependence of Fano Resonances in Single Molecules. *Phys. Chem. Chem. Phys.* **2017**, *19*, 6416–6421.

(65) Wang, X.; Bennett, T. L. R.; Ismael, A.; Wilkinson, L. A.; Hamill, J.; White, A. J. P.; Grace, I. M.; Kolosov, O. V.; Albrecht, T.; Robinson, B. J.; et al. Scale-up of Room-Temperature Constructive Quantum Interference from Single Molecules to Self-Assembled Molecular-Electronic Films. *J. Am. Chem. Soc.* **2020**, *142*, 8555–8560.

(66) Leary, E.; Zotti, L. A.; Miguel, D.; Márquez, I. R.; Palomino-Ruiz, L.; Cuerva, J. M.; Rubio-Bollinger, G.; González, M. T.; Agrait, N. The Role of Oligomeric Gold-Thiolate Units in Single-Molecule Junctions of Thiol-Anchored Molecules. *J. Phys. Chem. C* **2018**, *122*, 3211–3218.

(67) Cabosart, D.; El Abbassi, M.; Stefani, D.; Frisenda, R.; Calame, M.; Van der Zant, H. S. J.; Perrin, M. L. A Reference-Free Clustering Method for the Analysis of Molecular Break-Junction Measurements. *Appl. Phys. Lett.* **2019**, *114*, No. 143102.

(68) Leary, E.; Kastlunger, G.; Limburg, B.; Rincón-García, L.; Hurtado-Gallego, J.; González, M. T.; Bollinger, G. R.; Agrait, N.; Higgins, S. J.; Anderson, H. L.; et al. Long-Lived Charged States of Single Porphyrin-Tape Junctions under Ambient Conditions. *Nano-scale Horiz.* **2021**, *6*, 49–58.

(69) Garner, M. H.; Solomon, G. C.; Strange, M. Tuning Conductance in Aromatic Molecules: Constructive and Counteractive Substituent Effects. *J. Phys. Chem. C* **2016**, *120*, 9097–9103.

(70) Liu, X.; Sangtarash, S.; Reber, D.; Zhang, D.; Sadeghi, H.; Shi, J.; Xiao, Z. Y.; Hong, W.; Lambert, C. J.; Liu, S. X. Gating of Quantum Interference in Molecular Junctions by Heteroatom Substitution. *Angew. Chem. Int. Ed.* **2017**, *56*, 173–176.

(71) Alanazy, A.; Leary, E.; Kobatake, T.; Sangtarash, S.; González, M. T.; Jiang, H.-W.; Bollinger, G. R.; Agrait, N.; Sadeghi, H.; Grace, I.; et al. Cross-Conjugation Increases the Conductance of Meta-Connected Fluorenones. *Nanoscale* **2019**, *11*, 13720–13724.

(72) Zotti, L. A.; Leary, E. Taming Quantum Interference in Single Molecule Junctions: Induction and Resonance Are Key. *Phys. Chem. Chem. Phys.* **2020**, *22*, 5638–5646.